Oxid Met (2011) 75:27–39
DOI 10.1007/s11085-010-9218-2

ORIGINAL PAPER

Effect of Pre-Oxidation at 800 °C on the Pitting Corrosion Resistance of the AISI 316L Stainless Steel

H. Buscail · S. El Messki · F. Riffard · S. Perrier · C. Issartel

Received: 24 August 2009 / Revised: 14 July 2010 / Published online: 30 September 2010

Abstract In situ X-ray diffraction was used to identify the oxides formed on the AISI 316L (containing 2% Mo) stainless steel during isothermal oxidation at 800 °C, in air. Good oxidation behavior was observed on this steel when considering kinetics, structural characteristics and scale adherence. It was demonstrated that molybdenum plays a protective role in that it hinders the outward iron diffusion and leads to the lower growth rate and the better scale adherence. The oxide scale was then composed of Cr_2O_3 with a small amount of $Mn_{1,5}Cr_{1,5}O_4$ at the external interface. Pre-oxidation of the AISI 316L also improved its aqueous corrosion resistance. No pitting corrosion occured during the corrosion test. Aqueous corrosion testing also showed that the oxide scale formed at 800 °C is crack-free and still adherent after cooling to room temperature.

Keywords AISI 316L · In situ X-ray diffraction (XRD) · Oxidation · Molybdenum

Introduction

The AISI 316L stainless steel is a technologically important material widely used in various sectors of industry due to its good corrosion resistance at high temperatures [1–6]. It has been shown that 100 h oxidation, in air, at 700 °C leads to the presence of Cr_2O_3 and Fe_2O_3 protuberant areas in the oxide scale [7]. On injection molding AISI 316L the steel porosity not only increased the kinetics of the corrosion process, but also determined the nature of the resulting oxide layer with more iron oxides formation [8]. Concerning the effect of reactive elements, it has been proposed that cerium and niobium additions lead to better oxidation resistance during isothermal

H. Buscail (✉) · S. El Messki · F. Riffard · S. Perrier · C. Issartel
LVEEM, Laboratoire Vellave sur l'Elaboration et l'Etude des Matériaux, EA 3864, Université de Clermont Ferrand, 8 rue J.B. Fabre, BP 219, 43006 Le Puy-en-Velay, France
e-mail: buscail@iut.u-clermont1.fr

oxidation at 700 °C, in dry air [9]. Yttria addition also leads to an increased oxidation resistance at 800 °C [10]. Moreover, other studies show that titanium coatings [11–14] or laser surface modification can be applied on AISI 316L materials for improved tribological properties [15, 16]. After oxidation at 900 °C, X-ray diffractograms [17] seem to show the presence of $NiFe_2O_4$, Fe_2O_3 and/or $(Fe_{0.6}Cr_{0.4})_2O_3$. Depending on the application, such materials are subjected to corrosive atmospheres and thermal cycling. Several studies [1–6] highlighted that, at high temperature, chromia-forming alloys such as AISI 316L stainless steels present an oxide growth leading mainly to chromia Cr_2O_3 and spinel type oxide formation. However, in situ X-ray diffraction (XRD) studies have never been performed on AISI 316L specimens at 800 °C in order to check if a change in the structural composition of the layer appears with time and if oxide phase transitions occur during cooling to room temperature as it was demonstrated on a AISI 304 substrate [18]. From the literature, it appears that pre-oxidation of the AISI 316L SS has been tested in order to improve its aqueous corrosion resistance [19–24]. A general corrosion improvement of this material was also obtained for biomedical applications [25–32]. In this case the objective is to avoid the hexavalent chromium release from the AISI 316L stainless steel implants [33]. On blank AISI 304 SS and AISI 316L SS specimens, cyclic voltammetry in sulfuric acid solution show that the native oxide layer on AISI 316L is more protective than on AISI 304 SS [34]. However, AISI 304 SS is sometimes preferred to the molybdenum grade AISI 316L because molybdenum tends to promote the formation of sigma phase, which is less resistant to nitric acid [35].

According to some authors [8] the AISI 316L oxidation is generally studied at temperatures lower than 900 °C and more frequently between 300 and 700 °C. In this temperature range the oxide scale appears to be composed of some iron containing oxides which are not considered as protective as chromia scales. Then, it is interesting to test this material in a higher temperature range in order to analyze the composition of the scale at testing temperature by in situ XRD. The aim of the present work is then to determine the oxidation mechanism of the AISI 316L SS at 800 °C, try to explain the good scale adherence and discuss the role played by molybdenum as an alloying element. Pitting corrosion tests were also performed in order to detect cracks in the oxide scale and estimate its protective character.

Experimental Procedures

The substrate material used in the present study was a grade AISI 316L austenitic stainless steel (SS) with the nominal chemical composition (in wt%): 17.7 Cr, 10.9 Ni, 2.16 Mo, 1.57 Mn, 0.55 Si, 0.023 C and balance Fe. It was compared with an AISI 304 SS: 17.9 Cr, 9.05 Ni, 0.15 Mo, 1.52 Mn, 0.47 Si, 0.053 C and Balance Fe.

Austenitic steel specimens, provided by ArcelorMittal-Imphy, were polished on SiC paper up to the 800 polishing grade, then washed with ethanol and finally dried just before isothermal oxidation at 800 °C.

The kinetics results under isothermal conditions were recorded by means of a Setaram TG-DTA 92-1600 microthermobalance, during 90 h, at 800 °C, in air.

The in situ characterization of the oxide scales was carried out in a high-temperature MRI chamber adapted on an X-ray Philips X' PERT MPD diffractometer (copper radiation, $\lambda k_\alpha = 0.154$ nm). The XRD conditions were 2Θ scan, step 0.1°, range from 10° to 90°, 4.5 s counting time. The heating-up rate was fixed at 30 °C/min. The morphology of the external interface, as well as the cross-sections, were observed with secondary electrons using a scanning electron microscope (SEM). The analysis of the scale was performed with the energy dispersive X-ray spectroscopy (EDS).

The pitting corrosion resistance of the samples was investigated by electrochemical potentio-dynamic tests. These tests were conducted in a conventional three-electrode cell using a Pt foil as the auxiliary electrode and a saturated calomel electrode (SCE) as the reference one. The working electrode was constructed using either non oxidized (blank) or pre-oxidized AISI 316L specimens of a cylindrical shape. The tests were initiated when steady-state open circuit potential was developed after 30 min (E_{oc}). The starting potential was taken as $E_{oc} - 250$ mV. The potential was swept in the anodic direction at 120 mV/min until the potential of 1500 mV/SCE was reached. Then, the scan was reversed in the cathodic direction until the $E_{oc} - 250$ mV. The electrolyte was a 9 g/l NaCl (pH 7) aerated solution at 37 °C. Each test was performed on ten different specimens in order to check the reproducibility.

Results

Kinetics

Thermogravimetric analysis was carried by exposure for 90 h, at 800 °C, in air. The mass gain curves per unit area are given in Fig. 1. With the AISI 304 SS the kinetics show parabolic behavior ($k_p = (2.7\pm 0.2) \times 10^{-13}$ g^2/cm^4/s) all along the oxidation test. On AISI 316L parabolic behavior is also observed all along the oxidation test ($k_p = (4 \pm 0.2) \times 10^{-14}$ g^2/cm^4/s). The oxidation rate is slightly lower with AISI 316L specimens compared to that for AISI 304 SS under the time and condition tested.

Scale Surface Morphology

The surface morphology of the scale formed on the AISI 316L oxidized during 90 h, in air, at 800 °C, is presented in Fig. 2. No scale spallation was observed. This scale exhibits large flat crystals and small grains. In order to analyze the scale composition, EDS analysis of the sample surface was performed (Fig. 3). It shows the presence of manganese, chromium, oxygen and a small amount of iron. The same composition is observed on both the flat crystals and the smaller grains present on the surface.

Scale Cross-Section Morphology

SEM examinations were carried out on the 316 SS cross-section (Fig. 4) in order to estimate the scale thickness and to identify the elements incorporated in the oxide scale. After 90 h oxidation at 800 °C, large flat crystals are observed at the external

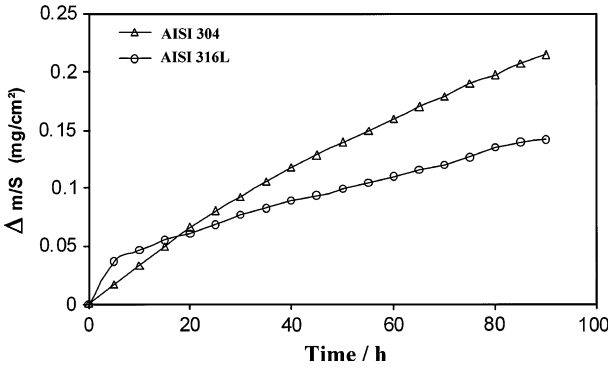

Fig. 1 Mass gain curve obtained during isothermal AISI 316L SS and AISI 304 SS oxidation, at 800 °C, in air

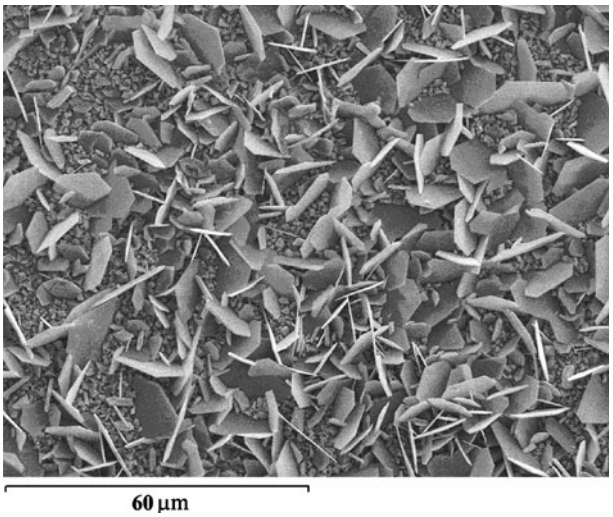

Fig. 2 SEM micrograph showing the morphology on the AISI 316L SS surface oxidized at 800 °C, in air, after 90 h

interface on the resin side. The compact chromia part of the scale is 3 ± 0.5 µm thick and it exhibits some internal oxidation with small pegs penetrating into the alloy.

EDS analyses performed on the cross-section are given on Table 1. Due to secondary electron yield variation with atomic number, we can also note the presence of silicon and molybdenum as dark areas at the internal interface and along the steel grain boundaries. It appears that molybdenum and silicon are mainly located close to the internal interface.

On oxidized AISI 304 specimens in air [36], the scale generally exhibits Fe_2O_3 and $FeCr_2O_4$ nodules on the surface and the oxide scale is not very adherent. Our results show that AISI 316L specimens behave much better from the stand points of scale structure and scale adherence.

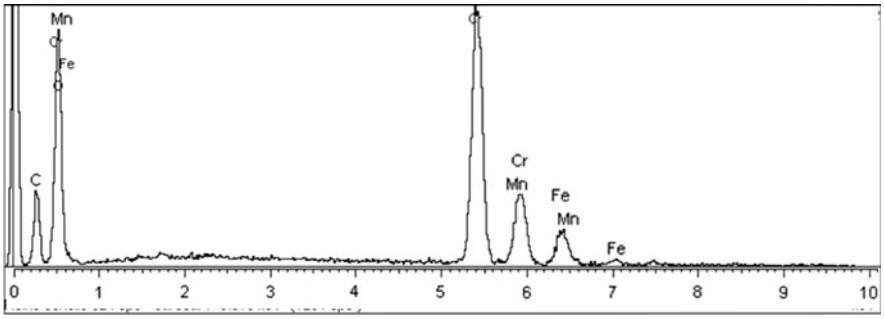

Fig. 3 EDS spectrum registered on the AISI 316L SS surface oxidized at 800 °C, in air, after 90 h

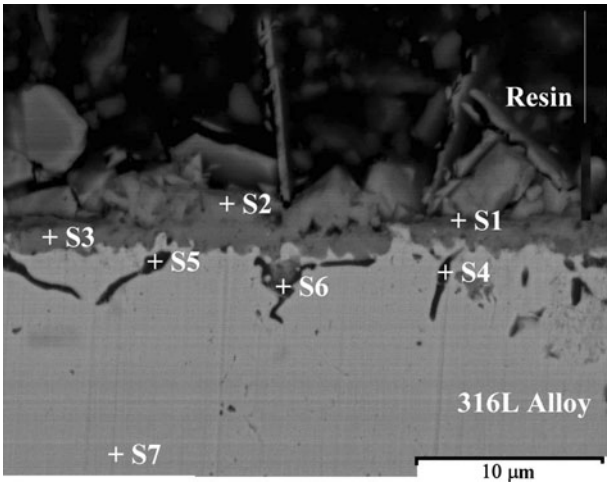

Fig. 4 SEM cross-section of the AISI 316L SS oxidized at 800 °C, in air, after 90 h (BSE imaging)

Table 1 EDS analysis obtained on the cross-section of the AISI 316L SS oxidized at 800 °C, in air, during 90 h

At.%	O	Si	Cr	Mn	Fe	Ni	Mo
S1	63.76	0.58	31.65	3.08	0.93		
S2	61.41	0.41	26.57	11.61			
S3	63.85	0.71	34.31		1.13		
S4	37.52	18.46	6.63		31.84	4.61	0.93
S5	51.93	2.68	29.87		13.18	1.98	0.36
S6	51.75	18.17	12.49	0.93	14.41	1.84	0.42
S7			13.19	0.88	72.80	11.58	

In Situ X-Ray Diffraction Results

The oxide scale formed on the AISI 316L was analyzed by in situ XRD on the metallic substrate at 800 °C, in air (Fig. 5). This figure shows the presence of the $Mn_{1.5}Cr_{1.5}O_4$ (JCPDS 33-0892) and Cr_2O_3 chromia (JCPDS 38-1479). It appears that both oxides nucleate and grow simultaneously on the specimen surface. The

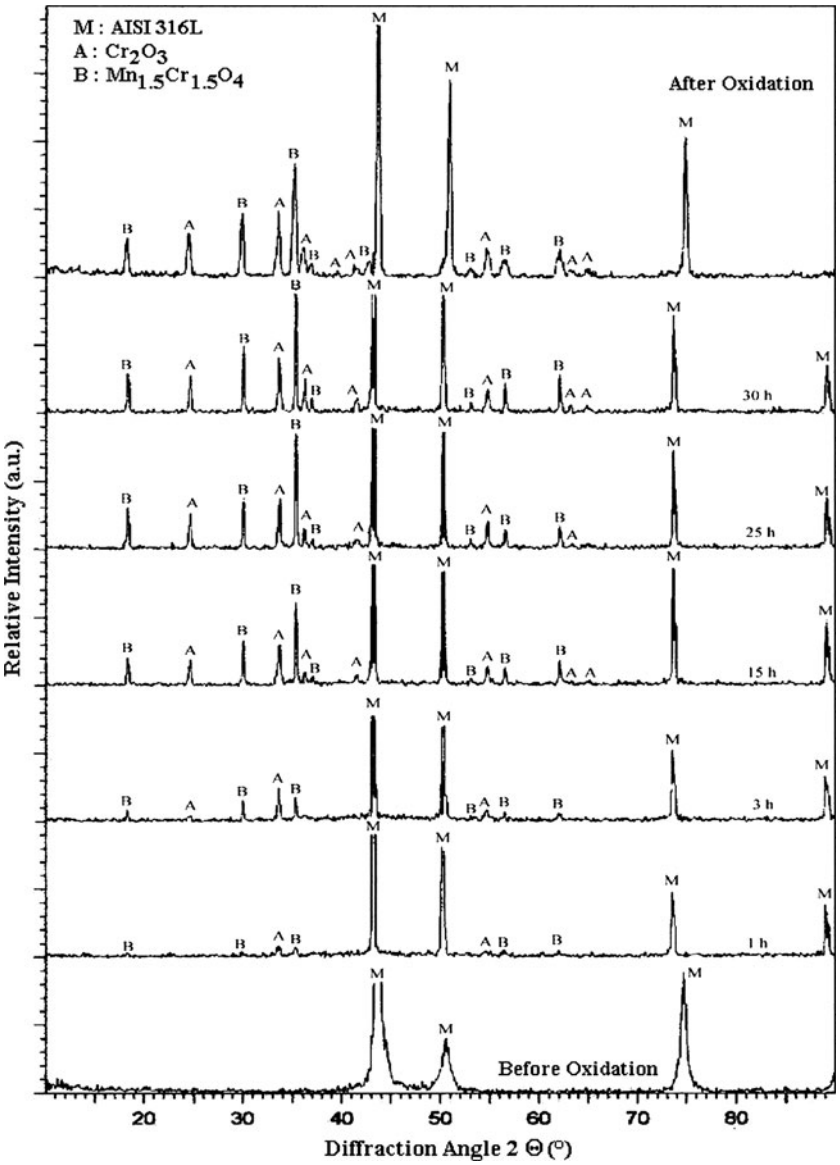

Fig. 5 In situ XRD patterns obtained on the AISI 316L SS during isothermal oxidation, at 800 °C, in air

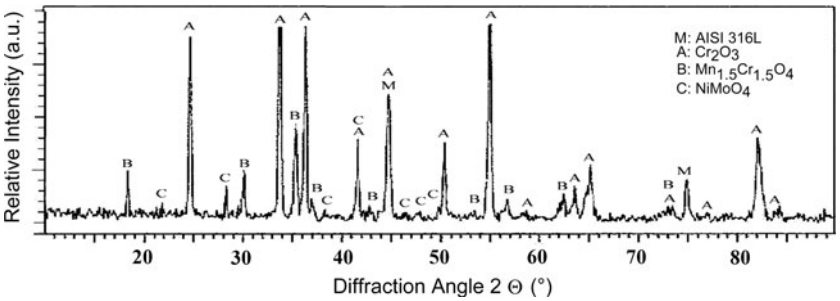

Fig. 6 XRD performed on the AISI 316L SS after 125 h oxidation at 800 °C, in air

relatively high $Mn_{1.5}Cr_{1.5}O_4$ peak intensities are not due to a higher proportion of this oxide in the scale but to the location of this oxide at the external interface.

Figure 6 also shows that the in situ XRD patterns obtained after 30 h oxidation is similar to the one obtained after cooling to room temperature. This indicates that no phase transition or scale spallation occurs during cooling to room temperature. Finally, the in situ XRD results show that no detectable iron-containing oxides are formed on AISI 316L specimens at 800 °C.

It further appears in Fig. 5 that no molybdenum-containing oxides could be detected on the XRD patterns at 800 °C after 30 h oxidation. In order to identify the molybdenum-containing oxides and better to explain the role of this element, XRD was performed after a longer exposure time (i.e., 125 h) (Fig. 6).

Figure 6 shows that molybdenum is detected as $NiMoO_4$ (JCPDS 33-0948) at 800 °C after 125 h oxidation. On AISI 304 specimens, a previous study that used in situ X-ray diffraction, showed that the oxide scale formed on this steel is composed of iron-containing oxides such as Fe_2O_3 and $FeCr_2O_4$. These oxides were responsible for the relatively bad oxidation behavior of AISI 304 at this temperature [36].

Cyclic Voltammetry

Anodic cyclic voltammetry curves of blank AISI 316L substrate and oxidised AISI 316L specimens at 800 °C in air, during 48 h, are shown on Fig. 7. On both specimens the pitting potential $E_{gp} = 720$ mV/SCE and the repassivation potential $E_{rep} = 0$ mV/SCE are close to each other despite the initial surface state. For the unoxidized substrate, a continuous increase of the current density has been observed for the entire range of potential. At 1500 mV/SCE the anodic current density value of about 2.9×10^{-3} A/cm^2. A lesser rate of dissolution was shown by the sample oxidized at 800 °C showing the lowest current density for the entire range of potential studied. At 1500 mV/SCE the anodic current density value of about 4.6×10^{-4} A/cm^2. Thus the protective character of the oxide layer is demonstrated by the current density variation which was one order magnitude lower for oxidized AISI 316L specimens.

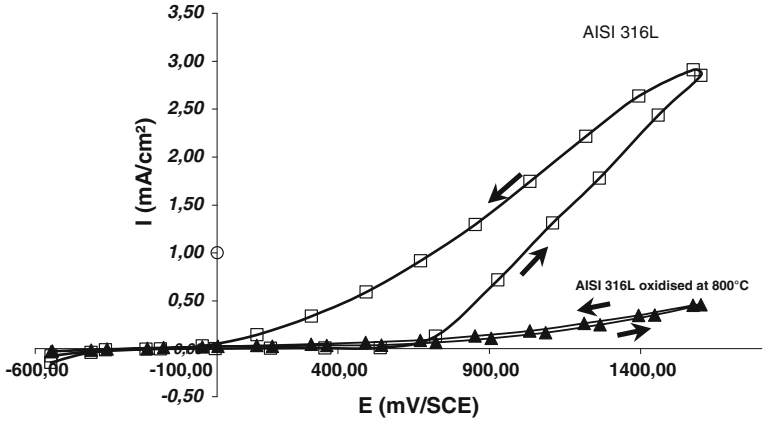

Fig. 7 Cyclic voltammetry (in aerated 9 g/l NaCl solution) of: the AISI 316L SS (unoxidized) and the AISI 316L oxidized 48 h at 800 °C, in air

Discussion

The main kinetics results obtained on the AISI 316L SS between 800 at 1000 °C are given in Table 2. The parabolic behavior was always encountered in this temperature range. This permitted the calculation of the parabolic rate constants k_p at each temperature.

The Arrhenius plots of the k_p values gives an activation energy (E_a) calculated from the slope of the curve which is found to be $E_a = 197 \pm 30$ kJ/mol. This value is close to those obtained in the literature during the oxidation of chromia-scale (Cr_2O_3) forming alloys. According to some authors [37, 38], E_a is ranges between 250 and 290 kJ/mol. This activation energy is in good agreement with the SEM cross-section observation (Fig. 4) and in situ XRD (Fig. 5), which showed that the scale was composed of a continuous chromia scale. The good oxidation behavior is also due to the absence of iron-containing oxides owing to the presence of silica and $NiMoO_4$ close to the internal interface (Fig. 4). XRD and EDS analysis sowed that no iron containing oxides where found in the oxide scale formed at 800 °C compared to what was proposed by some authors after oxidation at 900 °C [17].

The scale cross-section also revealed that the oxide scale was adherent to the substrate. Silicon and molybdenum were been found at the metal/oxide interface (Table 1). Our results obtained at 800 °C are comparable to those of Sobral et al. [8], who studied the oxidation of AISI 316L SS between 700 and 900 °C. He also

Table 2 k_p Values obtained on the AISI 316L between 800 at 1000 °C

	AISI 316L k_p ($g^2\ cm^{-4}\ s^{-1}$)
800 °C	4×10^{-14}
900 °C	1.9×10^{-13}
1000 °C	2.56×10^{-12}

showed the presence of $(Mn_{1.5}Cr_{1.5})O_4$ and Cr_2O_3 after long exposure tests at 900 °C.

Role of Silicon and Molybdenum on the Oxidation Mechanism

Few studies have discussed the role of molybdenum on the corrosion behavior of a Cr_2O_3-scale former at high temperatures. Molybdenum is generally added into the 316L steel as a solid-solution strengthener. But with respect to the oxidation resistance, molybdenum can be undesirable because MoO_3 tends to volatilize or melt even at moderate a temperature [7].

By contrast, silicon has been more extensively examined on chromia forming alloys, as a protective element. Even though too high an amount of silicon is considered as detrimental for the steels mechanical properties [39], its addition generally improves oxidation resistance. Some authors [40–42] stated that silicon segregates at the oxide/alloy interface and blocks the iron cationic diffusion. Silicon is then supposed to be present as a silica film, which lowers the steel oxidation rate. The high oxygen affinity of silicon, permit its internal oxidation, developing SiO_2 precipitates at the internal interface [43, 44]. Then, it is reported that silica acts as a diffusion barrier and leads to peg the chromia scale on the substrate [45, 46]. Silica will also lower the porosity at the internal interface acting as vacancies sinks [47]. Silicon also reduces the amount of non-protective iron oxides inside the scale [48] and hinders the iron rich nodule formation [41].

Influence of the Silicon Content

Paùl and coworkers have shown that during the oxidation of a AISI 304 type stainless steel between 900 and 1000 °C, a maximum 0.88% (wt%) silicon content leads to the formation of a chromia scale even at 1000 °C. It should be noticed that they studied a manganese free substrate and that the comparison with manganese containing steels is then not very easy [49]. On the other hand, it appears that a too high amount of silicon induces more scale spallation between the alloy and the silica scale or at the silica/chromia interface [42]. It is the reason why silicon is rarely added at more than 1 wt%. One should also take care that the chromium presence is necessary to avoid the fayalite Fe_2SiO_4 formation, which is a very bad diffusion barrier [50, 51]. Effectively, according to Stott, the necessary amount of silicon needed to the SiO_2 formation can be lower when the chromium content increases [51].

Concerning higher silicon additions, the paper of Li and Gleeson [52] compared the oxidation behavior of Ni-base alloys with and without about 2.7 wt% Si addition at 1000 °C. From oxidation results of the cast model alloys, Si addition was found to improve oxidation resistance by forming a continuous SiO_2 layer at the alloy scale interface, which resulted in decreased oxidation kinetics. The cast alloys with Si addition also showed larger average effective inter-diffusion coefficients of chromium compared to the cast alloys without Si addition. As a consequence, the Si addition assisted in the establishment and re-formation of a chromia scale during oxidation. In the case of the wrought commercial alloys a discontinuous distribution

of SiO_2 precipitates in the vicinity of the alloy/scale interface was found to be beneficial to cyclic oxidation resistance. In the present work the alloy silicon content is much lower and the substrates are iron-base steels. Nevertheless, the molybdenum content is close to 2 wt% in the 316L SS and should be taken into account.

Role of Molybdenum

At 800 °C, cross-sectional examination showed that molybdenum is associated with silicon at the internal interface (Fig. 4). These two elements seem to show similar oxidation and diffusion behavior. The low outward silicon diffusion through the oxide scales is a well-known phenomenon [53], and our results indicate that molybdenum shows a similar behavior at low temperature. At 800 °C, molybdenum is found close to the oxide/steel interface (Fig. 4) and $NiMoO_4$ is detected by XRD. In our study, it should be noticed that at 800 °C the temperature seems to be low enough to permit the $NiMoO_4$ detection by XRD after cooling to room temperature (Fig. 6). No evaporation of molybdenum oxide (MoO_3) occurs during the oxidation process at 800 °C [7].

The good scale adherence observed, can be due to the fact that molybdenum and silicon oxides could fill the vacancies generated at the internal interface by the outward chromium and manganese cation diffusion through the oxide scale. It is known that at low temperatures the volume fraction of MoO_3 is 340% compared to molybdenum and the volume fraction of SiO_2 is 180% larger than silicon [54–57]. This phenomenon can contribute to hinder the outward iron diffusion from the substrate. It has been also proposed that a Mo-Si–O amorphous phase (not detectable by XRD) could form instead of SiO_2 and will show better protective properties [58]. At 800 °C, the effect of an amorphous phase can be envisaged at the oxide/steel interface where molybdenum has been detected. Even though they contain similar silicon contents, AISI 316L shows a relatively better behavior compared with AISI 304 type steel at 800 °C, the chromia scale adherence is improved and no iron containing oxides are formed (Fig. 4). This is certainly due to the 2% molybdenum content of the AISI 316L SS. This element can be added with a relatively high content compared to the 0.5% silicon generally introduced in stainless steel. Then, 2% molybdenum shows a quantitative effect on the AISI 316L oxidation protection without the over-doping effects encountered with the highest silicon containing steels [42].

On oxidized specimens, the protective character of the oxide layer is demonstrated by the pitting corrosion tests. Then, the current density variation is one order magnitude lower for oxidized AISI 316L specimens compared to blank specimens. Our results are in accordance with the literature which shows that pre-oxidation of the AISI 316L improves its aqueous corrosion resistance for biomedical applications [19–32]. In this case the objective is to avoid the hexavalent chromium release from the AISI 316L stainless steel implants [33]. Our results also show that no pitting corrosion occurs during the test. It then indicates that the oxide scale formed at 800 °C is crack free and still adherent after cooling to room temperature.

Conclusions

In the present work, in situ X-ray diffraction was used to identify the oxides formed on the AISI 316L stainless steel during isothermal oxidation at 800 °C, in air. It showed the presence of the $Mn_{1.5}Cr_{1.5}O_4$ (JCPDS 33-0892) and Cr_2O_3 chromia (JCPDS 38-1479). It also appeared that both oxides nucleate and grow simultaneously on the specimen surface. According to the SEM cross-section observations, it appeared that the relatively high $Mn_{1.5}Cr_{1.5}O_4$ peak intensities are not due to a higher proportion of this oxide in the scale but to the location of this oxide at the air/scale interface. No phase transition or scale spallation occured during cooling to room temperature. The results showed that no iron-containing oxides formed on AISI 316L specimens at 800 °C.

Our results were compared with those obtained on AISI 304 SS in order to better explain the role of molybdenum on the oxidation process of AISI 316L SS (containing 2% Mo). Good oxidation behavior of the AISI 316L SS was observed when considering kinetics and structural characteristics. It was shown that molybdenum plays a protective role, as it is observed with silicon. Moreover, it is possible to add a higher content of molybdenum (2%) in the stainless steel compared with silicon (usually 0.5%). This higher protective-element content hinders the outward diffusion of iron and leads to the lower growth rate and the better scale adherence observed. The oxide scale was then composed of Cr_2O_3 with a small amount of $Mn_{1,5}Cr_{1,5}O_4$ at the external interface. The better scale adherence observed is inferred to be due to the fact that molybdenum and silicon oxides could fill the vacancies generated at the internal interface by the outward chromium and manganese cation diffusion through the oxide scale. At 800 °C, Mo is mainly located, as $NiMoO_4$, close to the alloy/oxide interface. Our results also show that no pitting corrosion occurs during the corrosion test. Pre-oxidation of the AISI 316L improves its aqueous corrosion resistance. Pitting corrosion tests also show that the oxide scale formed at 800 °C is crack free and still adherent after cooling to room temperature.

References

1. J. Pitter, F. Cerny, J. Cizner, J. Suchanek, and D. Tischler, *Surface and Coatings Technology* **200**, 73 (2005).
2. S.-G. Kim, M.-Z. Hong, S. P. Yoon, J. Han, S. W. Nam, T. H. Lim, and S.-A. Hong, *Journal of Sol–Gel Science and Technology* **28**, 297 (2003).
3. J. E. Indacochea, J. L. Smith, K. R. Litko, E. J. Karell, and A. G. Raraz, *Oxidation of Metals* **55**, 1 (2001).
4. A. A. Syed, T. A. Denoirjean, P. Fauchais, and J. C. Labbe, *Surface and Coatings Technology* **200**, 4368 (2006).
5. C. Vernault and J. Mendez, *Annales de Chimie Sciences et Matériaux* **24**, 351 (1999).
6. A. L. Johnson, D. Parsons, J. Manzerova, D. L. Perry, D. Koury, B. Hosterman, and J. W. Farley, *Journal of Nuclear Materials* **328**, 88 (2004).
7. X. Wang, L. Wang, M. Zhu, J. Zhang, and M. Lei, *Transactions of Nonferrous Metals Society of China* **16**, 676 (2006).

8. A. V. C. Sobral, M. P. Hierro, F. J. Pérez, W. Ristow Jr., and C. V. Franco, *Materials and Corrosion* **51**, 791 (2000).
9. S. K. Samanta, S. K. Mitra, and T. K. Pa, *Materials Science and Engineering A* **430**, 242 (2006).
10. A. Bautista, F. Velasco, and J. Abenojar, *Corrosion Science* **45**, 1343 (2003).
11. D. Siva Rama Krishna and Y. Sun, *Surface and Coatings Technology* **198**, 447 (2005).
12. D. Siva Rama Krishna and Y. Sun, *Applied Surface Science* **252**, 1107 (2005).
13. P. Furman, J. Gluszek, and J. Masalski, *Journal of Materials Science Letters* **16**, 471 (1997).
14. M. Vigen Karimi, S. K. Sinha, D. C. Kothari, A. K. Khannab, and A. K. Tyagic, *Surface and Coating Technology* **158–159**, 609 (2002).
15. R. Singh and N. B. Dahotre, *Journal of Materials Science* **40**, 5619 (2005).
16. P. S. N. Stokes, F. H. Stott, and G. C. Wood, *Materials Science and Engineering A* **121**, 549 (1989).
17. A. Bautista, F. Velasco, M. Campos, M. E. Rabanal, and J. M. Torralba, *Oxidation of Metals* **59**, 373 (2003).
18. N. Karimi, F. Riffard, F. Rabaste, S. Perrier, R. Cueff, C. Issartel, and H. Buscail, *Applied Surface Science* **254**, 2292 (2008).
19. F. S. Shieu, M. J. Deng, and S. H. Lin, *Corrosion Science* **40**, 1267 (1998).
20. A. I. Almarshad and D. Jamal, *Journal of Applied Electrochemistry* **34**, 67 (2004).
21. O. H. Kwon, S.-H. Ahn, J.-G. Kim, and J.-G. Han, *Journal of Materials Science Letters* **21**, 41 (2002).
22. C. Carboni, P. Peyre, G. Beranger, and C. Lemaitre, *Journal of Materials Science* **37**, 3715 (2002).
23. M. F. Montemor, M. G. S. Ferreira, N. E. Hakiki, and M. Da Cunha Belo, *Corrosion Science* **42**, 1635 (2000).
24. W. H. Dickinson, Z. Lewandowski, and R. D. Geer, *Corrosion* **52**, 910 (1996).
25. D. J. Blackwood, *Corrosion Reviews* **21**, 97 (2003).
26. C.-C. Shih, C.-M. Shih, Y.-Y. Su, L. H. J. Su, M.-S. Chang, and S.-J. Lin, *Corrosion Science* **46**, 427 (2004).
27. Y. Tomizawa, T. Hanawa, D. Kuroda, H. Nishida, and M. Endo, *J. Artif. Organs* **9**, 61 (2006).
28. M. L. Roemhildt, T. D. McGee, and S. D. Wagner, *Journal of Materials Science: Materials in Medicine* **14**, 137 (2003).
29. L. M. Weldon, P. E. Mchugh, W. Carroll, E. Costello, and C. O'Bradaigh, *Journal of Materials Science: Materials in Medicine* **16**, 107 (2005).
30. J. Beddooes, and K. Bucci, *Journal of Materials Science: Materials in Medicine* **10**, 389 (1999).
31. G. Rondelli, B. Vicenti, and A. Cigada, *British Corrosion Journal* **32**, 193 (1997).
32. K. Bordji, J. Y. Jouzeau, D. Mainard, E. Payan, J. P. Delagoutte, and P. Netter, *Biomaterials* **17**, 491 (1996).
33. M. do Carmo Pereira, M. do Lourdes Pereira, and J. P. Sousa, *BioMetals* **12**, 275 (1999).
34. Z. Kerner, A. Horvath, and G. Nagy, *Electrochimica Acta* **52**, 7529 (2007).
35. G. Suresh, V. R. Raju, U. Kamachi Mudali, and R. K. Dayal, *Corrosion Engineering Science and Technology* **38**, 309 (2003).
36. N. Karimi, PhD thesis, Blaise Pascal University, Clermont-Ferrand, France (2007).
37. Y. P. Jacob, V. A. C. Haanappel, M. F. Stroosnijder, H. Buscail, P. Fielitz, and G. Borchardt, *Corrosion Science* **44**, 2027 (2002).
38. J. H. Chen, P. M. Rogers, and J. A. Little, *Oxidation of Metals* **47**, 381 (1997).
39. F. Armand and J. H. Davidson, in *Les aciers inoxydables*, eds. P. Lacombe, B. Baroux, and G. Beranger (Les Editions de Physique, Les Ulis, 1990).
40. A. M. Huntz, *Material Science and Engineering A* **201**, 211 (1995).
41. S. N. Basu and G. J. Yurek, *Oxidation of Metals* **36**, 281 (1991).
42. H. E. Evans, D. A. Hilton, R. A. Holm, and S. J. Webster, *Oxidation of Metals* **19**, 1 (1983).
43. M. Landkof, A. V. Levy, D. H. Boone, R. Gray, and E. Yaniv, *Corrosion Science* **41**, 344 (1985).
44. G. Aguilar, J. P. Larpin, and J. C. Colson, *Mémoires et Etudes Scientifiques-Revue de Métallurgie* **juillet/août**, 1992 (447).
45. S. Seal, S. K. Bose, and S. K. Roy, *Oxidation of Metals* **41**, 139 (1994).
46. R. N. Durham, B. Gleeson, and D. J. Young, *Oxidation of Metals* **50**, 139 (1998).
47. H. Nagai, *Materials Science Forum* **43**, 75 (1989).
48. F. J. Pérez, M. J. Cristobal, M. P. Hierro, and F. Pedraza, *Surface and Coatings Technology* **120–121**, 442 (1999).
49. A. Paúl, S. Elmrabet, L. C. Alves, M. F. da Silva, J. C. Soares, and J. A. Odriozola, *Nuclear lnstruments and Methods in Physics Research B* **181**, 394 (2001).

50. M. I. Manning, in *The influence of oxide scale fractures on the high temperature oxidation behaviour of steel*, eds. (Deutshe Gesellscaft für Metallkunde eV, Oberursel, West Germany, 1983), p. 283.
51. F. H. Stott, G. C. Wood, and J. Stringer, *Oxidation of Metals* **44**, 113 (1995).
52. B. Li and B. Gleeson, *Oxidation of Metals* **65**, 101 (2006).
53. Y. Q. Liu, G. Shao, and P. Tsakiropoulos, *Intermetallics* **9**, 125 (2001).
54. G. H. Meier, *Oxidation of Intermetallics* **12**, 779 (2004).
55. T. C. Chou and T. G. Nieh, *Scripta Metallurgica et Materialia* **26**, 19 (1992).
56. T. C. Chou and T. G. Nieh, *Scripta Metallurgica et Materialia* **27**, 1637 (1992).
57. T. C. Chou and T. G. Nieh, *Journal of Materials Research* **8**, 1605 (1993).
58. K. Yanagihara, K. Przybylski, and T. Mauryama, *Oxidation of Metals* **47**, 277 (1997).